JOURNAL OF GEOPHYSICAL RESEARCH, VOL. 100, NO. A7, PAGES 12,151–12,161, JULY 1, 1995

Ponderomotive effects on distributions of O^+ ions in the auroral zone

E. Witt, M. K. Hudson, and X. Li

Physics and Astronomy Department, Dartmouth College, Hanover, New Hampshire

I. Roth and M. Temerin

Space Sciences Laboratory, University of California, Berkeley

Abstract. Test particle calculations are used to compute the effects of gravity and ponderomotive acceleration by shear Alfvén wave oscillations on the distribution function of O^+ ions along auroral field lines, assuming an ionospheric Maxwellian source of the ions at 2000 km altitude with ~0.5 eV of thermal energy in the parallel component of velocity. The electric field model corresponds to a standing wave oscillation with a frequency ~1 Hz in the azimuthal direction superimposed on the background dipole field, in which the wave amplitude is either increasing or decreasing in time. The electric field is taken to be primarily in the perpendicular direction. The time varying wave produces broad distributions with widths of 2 to 10 times the initial 0.5-eV thermal energy of the Maxwellian source, and the density and flux of upward going O^+ ions at one Earth radius are both enhanced in this model. The oxygen ion distribution functions at 1 R_E altitude resulting from interaction with waves whose amplitudes are increasing in time have a more gradual lower energy cutoff than do the distribution functions resulting from decaying waves. The high-energy part of the distribution functions in growing waves reflects the temperature of the Maxwellian source, while the high-energy part of the distributions resulting from decaying waves steepens with time, independent of the source temperature.

Introduction

The auroral zone has been identified as a major source region of terrestrial ions in the magnetosphere. In order to escape, however, ionospheric ions, especially O^+ ones, must be energized enough to overcome Earth's gravity and survive charge exchange with ambient hydrogen at higher altitudes. *Li and Temerin* [1993] have reported a new acceleration mechanism that can accelerate O^+ ions upward. This acceleration is by means of a ponderomotive effect of large-amplitude, low-frequency ($\omega < \Omega_i$) waves on auroral field lines. The ponderomotive force on a single species is given by (valid in SI or cgs units)

$$\mathbf{F}_p = \frac{e^2}{4m}\nabla\left(\frac{1}{\Omega^2-\omega^2}{E_\perp}^2 - \frac{1}{\omega^2}{E_\parallel}^2\right), \qquad (1)$$

where $\Omega = eB_0/m$ is the particle's local gyrofrequency, ω is the wave frequency, and $E_\perp$ and $E_\parallel$ are the perpendicular and parallel (with respect to $\mathbf{B_0}$) components of the electric field amplitude [*Li and Temerin*, 1993]. The wave electric field components include the wave magnetic field contribution through Faraday's law. Because of the first term in (1), if the wave frequency is below the cyclotron frequency, the ponderomotive force takes a different form from the usual expression describing electrons influenced by high-frequency radiation [*Chen*, 1974]. In particular, low-frequency pulsations of auroral field lines can result in upward acceleration of hydrogen and oxygen ions.

Several authors have demonstrated the importance of the ponderomotive force in different contexts. *Similon et al.* [1986] derived general expressions for the ponderomotive force and applied it to examining the stability of low-frequency plasma modes. *Allan et al.* [1990, 1991] and *Allan* [1992] performed simulations of cavity modes with a two-dimensional (2-D) fluid MHD code and explained the resulting density modifications in terms of the ponderomotive force. They applied their results to explaining modifications of plasma density that were seen in the simulations of pulsations on closed field lines. The conclusion was that geomagnetic pulsations or cavity modes could pile up density in the equatorial portion of closed field lines. *Allan* [1993] discussed the energization and adiabatic heating that might be observed on closed field lines in response to ULF waves. *Guglielmi et al.* [1993] also presented expressions for a ponderomotive force and applied them

Paper number 95JA00175.
0148-0227/95/95JA-00175$05.00

to estimate the effects of geomagnetic pulsations on accelerating ions upwards on closed or open field lines. They also concluded that pulsations could enhance the equatorial plasma density on closed field lines.

In this paper we compute how low-frequency oscillations of auroral field lines modify the escaping flux of O^+ ions, and we use test particle calculations to compute how this acceleration modifies the distribution functions of the O^+ ions at different altitudes and times. In particular, we compute the distribution of O^+ ions, as a function of energy parallel to the magnetic field, that would be seen at 1 R_E altitude (R_E=6380 km) at various times. The O^+ ions are subject to electromagnetic and gravitational forces, and are assumed to be injected from a 0.5-eV Maxwellian source at colatitude $\theta = 19.3°$, azimuth $\phi = 0°$, and at 2000 km altitude. The model wave field corresponds to a standing wave, shear oscillation of the field lines such as might be responsible for PiB oscillations [*Lysak*, 1988] or Pc 1 waves. A small value ($\sim 3 \cdot 10^{-5}$) is chosen for the ratio of the parallel to perpendicular electric field, comparable to that chosen by *Li and Temerin* [1993], so that the oscillating parallel electric field plays no significant role in the ion dynamics. Our focus differs from previous authors in that we are interested in directly computing the time-dependent distribution functions instead of fluid quantities, and we are interested in enhancements of escaping O^+ flux on open field lines. Although hydrogen is the majority species at 2000 km altitude and hydrogen ions experience the same acceleration (in our approximation) as oxygen ions, we concentrate on the oxygen ions because we are interested in explaining the enhancements of O^+ ion flux observed during disturbed times and because the relative enhancement due to the ponderomotive force is larger for oxygen.

In order to compute time varying distribution functions we have had to make a number of assumptions. The most important of these are (1) we specify a model wave field, (2) we choose a somewhat arbitrary location and form for our source distribution of O^+ ions, and (3) we ignore ambipolar effects. These assumptions and their justifications or explanations are discussed below. Together they allow specific distribution functions to be calculated at various times in wave fields whose amplitudes are growing or decaying in time.

Specifying a model field means that we do not start with a self-consistent oscillation, nor do we allow mass transport to modify the oscillations as they proceed, in contrast to the self-consistent fluid simulations of *Allan et al.* [1990, 1991]. The justification is that we choose a reasonable form and frequency for the wave fields, which in turn allows us to compute the evolved distribution functions. The results are quantitative to the extent that the induced density changes up the field line are small and the model wave fields are reasonable. At the very least we can compute qualitative differences in the distributions caused by pulsations that are turning on or turning off.

Choosing our source to be at 2000 km is a compromise between wanting ponderomotive effects to override other effects and our ignorance of exactly where and when other effects (such as perpendicular wave heating) might be important. For the model fields chosen the wave amplitude increases monotonically from zero at the Earth's surface to a limiting value by somewhere near 2000-3000 km altitude. Because the ponderomotive force is proportional to the gradient of the square of the effective $E \times B$ drift (and of the field amplitude) it too increases monotonically with altitude on the chosen field line. An optimum choice of source altitude would be dependent on wave amplitude (for our particular choice of amplitude the ponderomotive force overcomes gravity at 1200 km altitude) and on what other processes might be operating. We select a Maxwellian distribution from a variety of other possibilities in order to make concrete comparisons of fluxes and densities at different altitudes and times.

The neglect of ambipolar effects is justified in one sense and model-dependent in another. *Banks and Holzer* [1969] computed a model ionosphere including an ambipolar field, taking into account sources of ionization, losses due to charge exchange, and interactions between H^+, O^+, and He^+ and neutral atoms. They produced model O^+ density and velocity profiles assuming an ion temperature of 3000° K. The resulting mean velocities of 40-150 m s^{-1} between 2000 km and 7000 km altitude (shown in their Figure 4) are small compared to the several km s^{-1} speeds the ponderomotive acceleration can cause, and these effects are ignorable in our model. *Li and Temerin* [1993] have shown that certain wave modes and ratios of $E_\parallel/E_\perp$ might lead to a different force on the electrons and ions, and this could be another source of an ambipolar field. In this case, differential acceleration of hydrogen and oxygen would occur, creating the possibility of ion-ion instabilities. Because this is strongly dependent on the wave mode, a more complete treatment including this effect must await a more complete calculation of the waves responsible for acceleration. Our treatment, as those by *Allan et al.* [1990, 1991] and *Allan* [1992, 1993] implies an equal acceleration of hydrogen and oxygen ions and no resulting ion-ion instabilities.

The following section describes the electric field model employed. Following this we describe how the parallel-to-B distribution functions are computed. This method uses the computational result that the perpendicular velocities are accounted for by expressions for the $E \times B$ and polarization drifts, and that the magnetic moment defined by the remaining cyclotron motion about these drifts is conserved. After the discussion of numerical methods we present numerical results and a discussion followed by conclusions.

Electric Field Model

Lysak [1988] has presented analytical and numerical models of PiB oscillations. In response to injections of parallel current flow from the magnetosphere, standing-wave like oscillations can be set up between the highly conducting ionosphere and the steep gradient in Alfvén wave speed at higher altitudes. His

analytic model has various modes. The zeroth order mode monotonically increases from zero amplitude at the ionosphere to an almost constant value above 2000 km altitude. The radial dependence in our model is chosen to follow this zeroth order mode. The unperturbed magnetic field is taken to be a dipole field, which in Earth-centered spherical coordinates has the magnitude (in Tesla)

$$B = 3.1 \cdot 10^{-5}(R_E/r)^3(1 + 3\cos^2\theta)^{1/2} \quad (2)$$

where (r, θ, ϕ) are the usual spherical coordinates, r is measured relative to the center of the Earth, $\phi = 0°$ at midnight local time, positive eastward, and $\theta = 0°$ at the north pole. Using the dipolar coordinates

$$\alpha = \sin^2\theta(R_E/r), \quad \Phi = -\phi, \quad \delta = \cos\theta(R_E/r)^2 \quad (3)$$

the electric field model is chosen to be

$$E_\alpha(\mathbf{r}, t) =$$

$$E_{\max}\cos(k_\alpha(\alpha - \alpha_0))\left[1 - e^{-(r/R_E - 1)/0.1288}\right] \cdot T(t) \quad (4)$$

where the time dependence for a growing wave is

$$\begin{array}{lll} T(t) = & 0 & t \le 0 \\ T(t) = & (1 - \exp(-t/\tau))\sin\omega t & t > 0 \end{array} \quad (5)$$

and for a decaying wave is

$$\begin{array}{lll} T(t) = & \sin\omega t & t \le 0 \\ T(t) = & \exp(-t/\tau)\sin\omega t & t > 0 \end{array} \quad (6)$$

We choose these differing expressions for $T(t)$ because physically these oscillations are not present all the time and do grow and decay. We present expressions in Appendix B that describe the distributions when the wave amplitude is constant in time.

The other electric field components are given by

$$E_\delta(\mathbf{r}, t) = 2.857 \cdot 10^{-5} E_\alpha(\mathbf{r}, t), \quad E_\phi = 0 \quad (7)$$

In (4)–(6) we take $\tau = 100s$, $\alpha_0 = \sin^2\theta_0(R_E/r_0)$, $\theta_0 = 19.3°$, and $r_0 = R_E + 2000$ km. Except where otherwise stated, $E_{\max} = 200$ mV m^{-1}, $\omega = 2\pi$ rad s^{-1} and $k_\alpha = 3850.9$. This choice of k_α sets the perpendicular wavelength equal to 20 km at 300 km altitude and 55 km at 1 R_E altitude ($r = 2R_E$). The radial profile of the electric field amplitude is plotted in Figure 1. With this choice of parameters the radial dependence is weak between altitudes of 2000 km to 1 R_E; the amplitude rises from 0.91 to 1.00 of its maximum value. The wave magnetic field has only a ϕ component and is found by time integrating the curl of the wave electric field. Gravitational deceleration competes with wave acceleration of O^+ ions by the electromagnetic fields. In our model we use

$$\mathbf{g} = -\hat{r}\, 9.82(R_E/r)^2 \quad (8)$$

where the units are in meters per second squared.

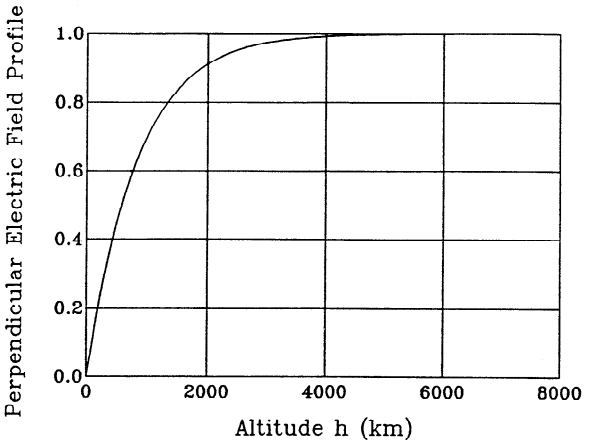

Figure 1. Radial profile from (4) of model electric field amplitude, normalized to the maximum amplitude. This profile rises from 0 at the Earth's surface to 0.91 at 2000 km altitude and asymptotes to unity at higher altitudes.

Method of Finding Parallel Distribution Function

The method of finding the parallel distribution function depends on the simulation result that the oxygen ions follow perpendicular drifts very closely with little additional energy added to cyclotron motion about these drifts. Furthermore, the ions remain approximately on their initial L shell. This means that the parallel distribution function can be computed using only the parallel velocity and the distance traveled along the field line. Oxygen ions are pushed from 1 R_E altitude where they span a region in phase space where the distribution is not known, backwards to 2000 km where the distribution function is known, thereby determining a transported region of phase space. An integral of the flux at 2000 km altitude yields the number of particles that fill the region at 1 R_E altitude, which then allows the average distribution function to be computed at 1 R_E as detailed below. The source of the O^+ ions at 2000 km altitude is assumed to be a Maxwellian with small perpendicular drifts, and the thermal energy of each velocity component of the source is taken to be 0.5 eV. Since the perpendicular drift at 2000 km can be up to 7 km s^{-1}, several times the 2.46 km s^{-1} thermal speed, the drift represents uniform translation of all ions back and forth in the azimuthal direction, and it is reasonable to assume that the ions have a small (0.5 eV) spread about this drift. Because no knowledge is assumed of what happens to the ions after they pass 1 R_E altitude, the computed distribution function consists only of ions that have an upward component of velocity at both 2000 km and 1 R_E altitudes. No downward going ions are included. This is the physical result when a strong enough ponderomotive force acts; all the ions initially launched upwards by the ionospheric source escape into the magnetosphere.

The solution for perpendicular drifts in a uniform magnetic field $\mathbf{B} = B_0\hat{z}$, and a sinusoidally oscillating

electric field amplitude $\mathbf{E} = (E_0 \sin\omega t)\hat{x}$ is

$$v_x = \frac{E_0}{B_0}\frac{\omega}{\Omega_i}\frac{\cos\omega t}{(1-\omega^2/{\Omega_i}^2)} + v_0\cos(\Omega_i t + \theta_p) \quad (9)$$

$$v_y = -\frac{E_0}{B_0}\frac{\sin\omega t}{(1-\omega^2/{\Omega_i}^2)} - v_0\sin(\Omega_i t + \theta_p) \quad (10)$$

where v_0 is an arbitrary velocity, θ_p an arbitrary phase constant, $\Omega_i = eB_0/m_i$ (in radians per second) is the ion cyclotron frequency, and ω is the wave frequency in radians per second. The velocity in the $\hat{x}$ direction corresponds to polarization drift plus cyclotron motion, and the velocity in the $\hat{y}$ direction corresponds to $E \times B$ drift plus cyclotron motion. The denominator becomes more important as the wave frequency approaches the cyclotron frequency. With the correspondence that x becomes α, and y becomes Φ in the dipolar (α, Φ, δ) coordinates, we have found that the perpendicular motion is well described by these drifts even as the amplitude of E and B change. Furthermore, the amplitude, v_0, of the cyclotron motion does not vary much from that which one would expect from conservation of the magnetic moment.

Time-integrating equations (9) and (10) yields the spatial excursion of the ions about the field lines. The oscillation in the azimuthal direction does not change the value of α, but the oscillation due to the polarization drift term (9) does change this coordinate. However, with the chosen electric field the amplitude of this oscillation (essentially $(E/B)/\Omega_i$) is 0.7 km at 1 R_E altitude, and 0.04 km at 2000 km altitude. Compared to the tens of kilometers perpendicular wavelength of the wave, both these excursions are ignorable and allow one to consider the α value or flux shell label constant.

Because the perpendicular motion basically follows (9) and (10), plus conservation of magnetic moment, and because the ions remain on their initial L shell, only the parallel velocity component and position along the field line as a function of time are needed for the ions in order to compute the parallel energy distribution. Appendix A describes how a point of the parallel velocity distribution is calculated.

As an illustration of the method, the parallel distribution of O^+ ions that would be seen at 1 R_E altitude in the absence of a wave is computed. These are ions that are launched from the Maxwellian source with enough energy to overcome the 2.7 eV gravitational potential energy barrier between 2000 km and 1 R_E altitudes. In this case conservation of magnetic moment and gravitational potential were used to find the arrival times and parallel velocities. The result is pictured in Figure 2.

In Appendix B we derive the theoretical time independent expression for the parallel distribution function $F(\mathcal{E}_\parallel, r, \mu)$ of ions on a given field line with the same magnetic moment μ, given a time independent potential energy difference $U(r)$ between a radius r on the field line and reference radius r_0 on the same field line. The analytical result is

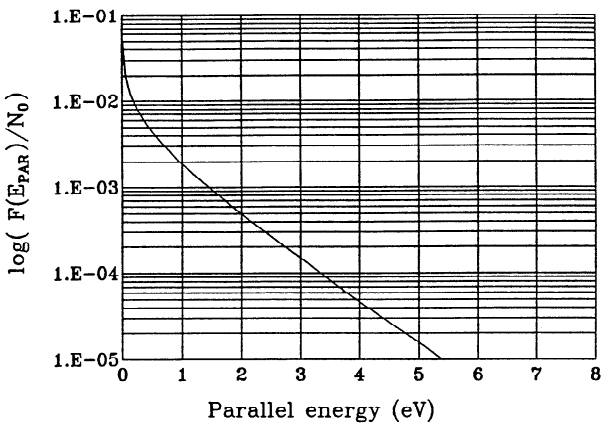

Figure 2. Computed parallel energy distribution of O^+ ions at 1 R_E altitude on a field line that passes through $\theta = 19.3°$ at 2000 km altitude, where a Maxwellian source with $T_\parallel$=0.5 eV is assumed. The computed distribution function agrees with the theoretical result (11) to one part in a thousand for $\mathcal{E}_\parallel$ >0.1 eV.

$$\frac{dn(\mathcal{E}_\parallel, r, \mu)}{d\mathcal{E}_\parallel} = F(\mathcal{E}_\parallel, r, \mu)$$

$$= \frac{n_0 B(r)}{2B_0\sqrt{2\pi {v_t}^2}}\frac{e^{-[\mathcal{E}_\parallel + \mu B(r) - \mu B_0 + U(r)]/(m_i {v_t}^2)}}{\sqrt{2m_i\mathcal{E}_\parallel}} \quad (11)$$

where n_0 is the number density of particles at a given μ at radius r_0,

$$0.5 m_i {v_t}^2 = T_\parallel \quad (12)$$

is the temperature associated with the parallel component of the Maxwellian distribution at r_0, B_0 is the magnetic field strength at r_0, and the parallel energy must satisfy:

$$\mathcal{E}_\parallel > \max(0, \mu B_0 - \mu B(r) - U(r)) \quad (13)$$

In the absence of waves, only gravity contributes to $U(r)$. We define the gravitational potential energy difference (in Joules) between r_0 and r to be $U_g(r)$:

$$U_g(r) = 9.82\, m_i\, R_E\left(\frac{R_E}{r_0} - \frac{R_E}{r}\right) \quad (14)$$

Integration of (11) over $\mathcal{E}_\parallel$ for upward going ions yields the density of upward going particles at any other point on the field line. For this example in the absence of waves and for $\mu = 0$ we find

$$n(r) = (n_0/2)\frac{B(r)}{B(r_0)}e^{-U_g(r)/(2T_\parallel)} \quad (15)$$

Equation (15) reduces to half the total density at $r = r_0$ because only the upward going ions are included.

For Figure 2 we choose $r_0 = R_E + 2000$ km , $r = 2R_E$, and choose the field line that passes through colatitude 19.3° at 2000 km altitude. The computed distribution function agrees with the theoretical expres-

sion (11) to better than one part in a thousand for $\mathcal{E}_{\|} > 0.1eV$. At $r = 2R_E$ the magnetic field ratio relative to 2000 km altitude is 1/3.6, the gravitational potential difference is 2.7 eV for O^+ ions, and (15) becomes

$$n(2R_E) = 0.138\, n_0\, e^{-2.72eV/(2T_{\|})} \qquad (16)$$

with $T_{\|}$ expressed in eV.

Numerical integration of the curve in Figure 2 yields $n(2R_E)/n_0 = 9.1 \cdot 10^{-3}$, in agreement with (16) when $T_{\|}$=0.5 eV. Comparison with a three-dimensional (3-D) distribution function is made in Appendix B.

When a wave is present, there is an effective ponderomotive potential. As was stated above, we find computationally that the magnetic moment is conserved, and the perpendicular velocities closely follow the modified $E \times B$ and polarization drifts. So we expect the computed distributions to resemble (11) when the potential energy now includes the ponderomotive potential, when the wave amplitude is constant in time. The 3-D distribution function in this case should be a Maxwellian with perpendicular drifts given by (9) and (10).

Results and Discussion

Figure 3 shows the computed parallel energy distribution function at 1 R_E altitude for three times after a standing wave has begun growing. The width of the horizontal scale is 16 eV for Figure 3a and 8 eV for Figures 3b and 3c. According to our assumptions the ions making up these distributions arrive at 1 R_E with 0.001 eV gyrational energy about their drifts, and the calculations show the particles leaving 2000 km altitude with less than 0.01 eV in cyclotron motion about their drifts.

At 450 s, the half width is about 6 eV, more than ten times the 0.5 eV thermal energy of the Maxwellian source. The half width decreases with time as lower energy particles have more time to be accelerated by the growing wave. Using an expression for the ponderomotive potential [*Li and Temerin*, 1993] $\Psi_p = -0.25 m_i (E_{\perp}/B)^2/(1-\omega^2/\Omega_i{}^2)$ (where the ponderomotive force is $-\nabla\Psi_p$) and the model electric field, one computes that Ψ_p varies from -2.01 eV at 2000 km to -32.2 eV at 1 R_E altitude. The difference in Ψ_p (-30.2 eV) together with the gravitational energy change of 2.72 eV gives a theoretical low-energy cutoff of 27.5 eV at large times. From Figure 3 we see that the peaks in the calculated distribution function approach this value with time. The slope of the distributions at 900 s and 1200 s at higher energies is close to that of the Maxwellian source at high energies. Assuming one unit per decade on the vertical scale, this slope is close to $(\log_{10}e)/(2T_{\|})$ at higher energies in agreement with (11), where for this case $T_{\|}$=0.5 eV.

The results for decaying waves are pictured in Figure 4, for a wave whose amplitude begins to decay at t=0. Distribution functions at 1 R_E at 100 s and 200 s after the wave begins to decay are displayed. In this

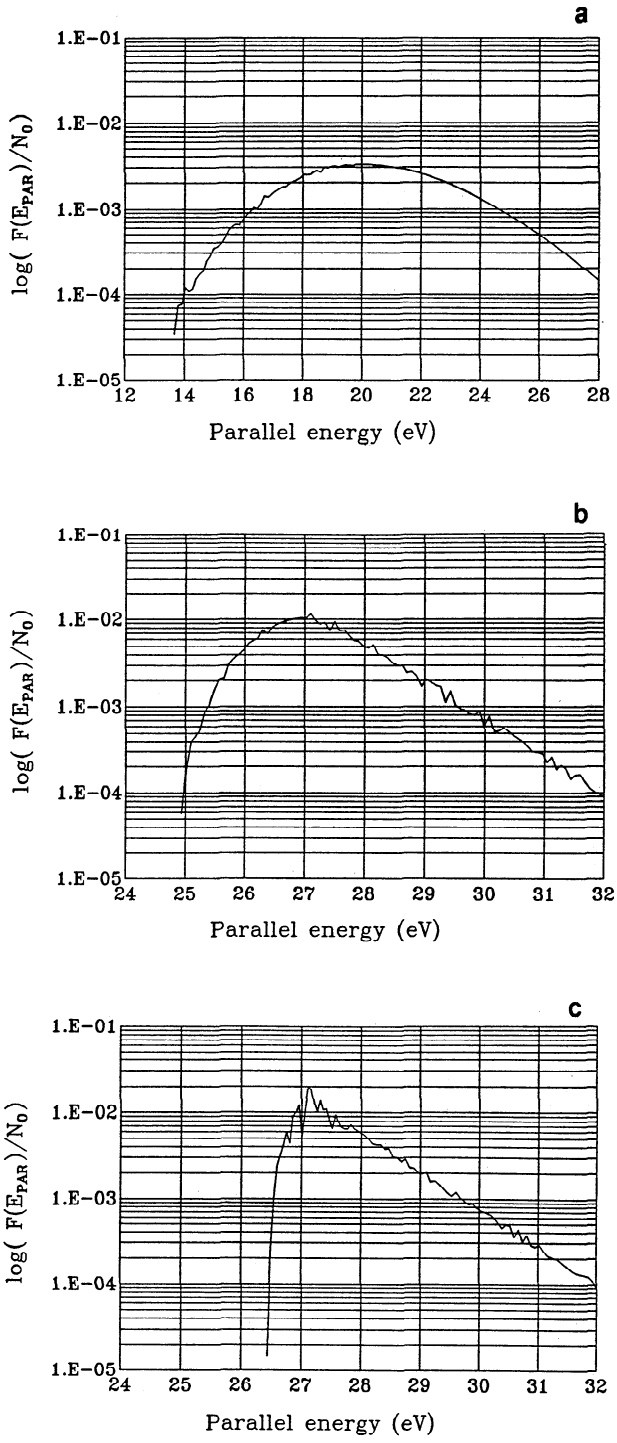

Figure 3. Computed parallel energy distribution of O^+ ions at 1 R_E altitude at (a) 450 s, (b) 900 s, and (c) 1200 s after a standing wave starts growing. The particles originate from a 0.5-eV Maxwellian source at $\theta = 19.3°$ and 2000 km altitude. The gyration energy about the perpendicular $E \times B$ and polarization drifts remains below 0.01 eV. Particles in the lower energy part of the curve leave 2000 km altitude up to several thousand seconds before the wave turns on. At 900 s and later, the slope of the high-energy part of the spectrum is $-0.43/(2T_{\|})$, where $T_{\|}$ is the thermal energy of the source.

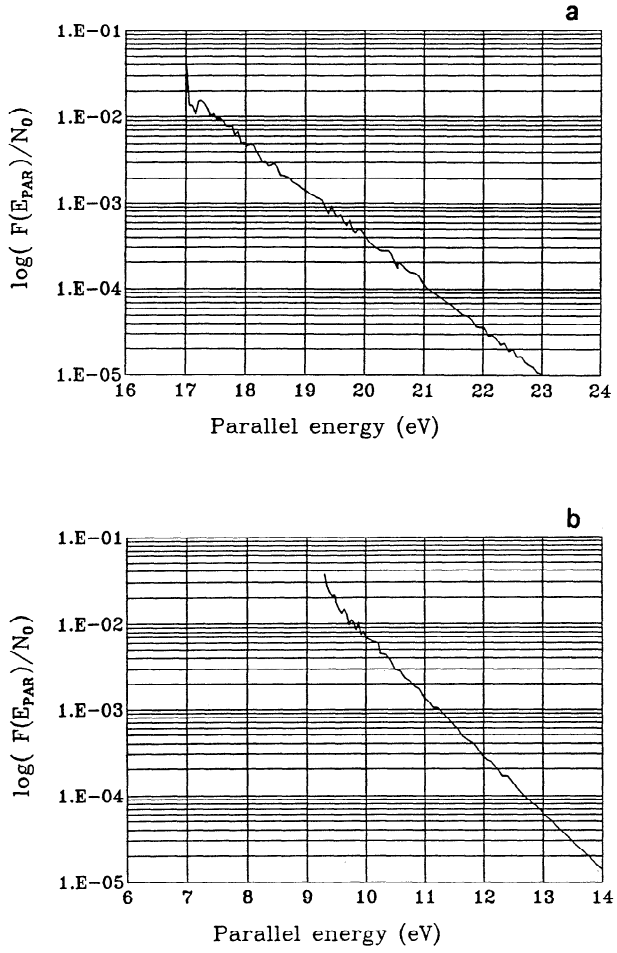

Figure 4. Computed parallel energy distribution of O^+ ions at 1 R_E altitude at (a) 100 s and (b) 200 s after the model electric field begins decaying. As for Figure 3, the particles originate from a source at 2000 km altitude, θ=19.3°, which is Maxwellian about the $E \times B$ and polarization drifts with a thermal energy of 0.5 eV. As in Figure 3, the gyrational energy about the perpendicular drifts remains less than 0.01 eV. In a decaying wave field the peak of the distribution shifts to lower energies at later times, and the spectrum grows steeper with time.

case there is a very sharp low-energy cutoff. Because the waves have been turned on for a long time, all of the lower energy particles have been accelerated past some minimum potential drop. The location of this low-energy cutoff decreases as the wave amplitude decreases. Note that the slope of the higher energy portion of the curve increases at later times. The principal differences between these spectra and those for growing waves are the nature of the low-energy cutoff (sharper for decaying waves) and location of the maximum (at lower energy for decaying waves as time increases), and in the slope of the higher energy part of the spectrum (becoming steeper as opposed to asymptoting to a constant as time increases).

In order to see the effects of finite perpendicular energy, we computed two cases in which the perpendicular gyration energy at 1 R_E altitude was 0.05 eV and the associated perpendicular energy at the source at 2000 km altitude was 0.18 eV, due to conservation of magnetic moment. In one case the gyrophase was 0° (velocity in α direction), and in the other case the gyrophase was 90° (perpendicular velocity in azimuthal direction). Except for the low-energy end of the spectra, which is pushed to higher energies because of the mirror force, the spectra closely resemble those in the case with negligible gyrational energy at 1 R_E (Figure 3b). The areas under both of the curves (or the implied density ratio at 1 R_E) are also similar, as discussed below. These results demonstrate the insensitivity of the computed distributions to restricted choices of initial perpendicular energy explored here, consistent with the small thermal energy of the Maxwellian at 2000 km altitude and with (11).

An integral of the distribution over parallel energy yields the ratio of the density at 1 R_E to that at 2000 km, and this integral depends on the assumed source distribution. The results for the Maxwellian source with 0.5 eV of thermal energy in the parallel component of velocity are given in Table 1. The theoretical result (from (15) evaluated for $T_{\|}$= 0.5 eV) for the ratio in the absence of waves is $9.1 \cdot 10^{-3}$. The first Table entry is the numerical result which is in good agreement. An interesting result of the calculation is the amount by which the upward going O^+ density is increased above its ambient value at 1 R_E altitude due to the influence of the waves. The Table shows that the O^+ density is enhanced above its ambient value (the first Table entry) by a factor of 2.6 (at 900 s), then 2.0 (at 1200 s) in the growing wave. In other words, the density enhancement subsequently decreases as the growing wave imparts a greater velocity to particles and total flux is conserved. This factor of two increase in density would result in only a 30% change in the local Alfvén speed, and probably would not modify the standing wave by much. One case at 900 s for the growing wave was computed in which the source distribution had 0.25 eV of thermal energy in the parallel component of velocity. The density ratio $n(2R_E)/n_0$ was 0.0151 in this case, 58% lower than that for a 0.5-eV Maxwellian source. In this case, however, the ambient (no wave present) density at 1 R_E altitude is $6{\cdot}10^{-4}$ n_0 (from (15) with $T_{\|}$=0.25 eV), so the enhancement over the ambient value is a factor of 25. If the model wave were a consistent oscillation of the field line in this case, the modified density would be expected to drastically modify the mode, probably by reducing the oscillation where the density was increased. The main point here is that lower source temperatures can lower the ambient density at 1 R_E altitude, but the wave lifts the same amount of O^+ ions leading to a greater enhancement above the ambient.

It is also interesting to compare the table results to the theoretical formula that is valid for a time-independent wave amplitude. Such an expression valid for negative potential differences and finite magnetic moment is derived in Appendix B (equation (B7)). This is the asymptotic ratio in the growing wave at late times, and the beginning ratio at $t = 0$ in the decaying wave. The potential difference from 2000 km including gravity and the ponderomotive potential is -27.5 eV,

Table 1. Computed Ratio of Number Density at $r = 2R_E$ to the Number Density at $r = R_E + 2000$ km Altitude (n_0)

Time, s	$n(2R_E)/n_0$	$E_\perp(2R_E)$, eV	Gyrophase ($2R_E$), deg	Wave Amplitude
0	0.0091	0.000	0°	Growing
450	0.0218	0.001	0°	Growing
900	0.0235	0.001	0°	Growing
1200	0.0179	0.001	0°	Growing
900	0.0194	0.050	0°	Growing
900	0.0190	0.050	90°	Growing
100	0.0156	0.001	0°	Decaying
200	0.0153	0.001	0°	Decaying

Ratio given in terms of the function of time of observation relative to the time the wave amplitude begins to change, energy in cyclotron motion at 2 R_E, gyrophase at 2 R_E, and character of wave. A Maxwellian source with $T_\parallel$ =0.5 eV at 2000 km altitude is assumed.

and the magnetic field ratio is 1/3.6. The resulting value from (B7) is 0.0146, which is in moderately good agreement with the 100 s value, 0.0156, found for the decaying wave.

Even more important than the density enhancement is the enhancement in the escaping O^+ flux. In the absence of an accelerating potential, the escaping flux consists of O^+ ions in the tail of the Maxwellian that have enough energy to overcome the 7.9 eV of gravitational potential from 2000 km to infinity. With $T_\parallel$=0.5 eV, this escaping flux at 1 R_E is a small fraction ($3.7 \cdot 10^{-4}$) of the upward going flux at 2000 km (or 9.9 n_0 cm^{-2} s^{-1}, where n_0 is the number density of O^+ ions at 2000 km altitude in cm^{-3}). However, if the ponderomotive force at 2000 km altitude is greater than gravity, all of the upward moving ions at 2000 km escape. This is the case in our model when the waves have fully turned on. The ratio at 2000 km altitude of the ponderomotive force to gravitational force along the field line is 2.0. In fact, in our model the ponderomotive force exceeds gravity down to 1200 km altitude. The amplitude at 2000 km would have to drop by $2^{1/2}$ from 182 mV m^{-1} to 129 mV m^{-1} for gravity to balance the ponderomotive force at 2000 km. When the ponderomotive force equals or exceeds the gravitational force at 2000 km altitude, all ions at 2000 km escape, and their flux at 1 R_E is the upward flux at 2000 km modified by the magnetic field ratio that accounts for flaring of flux tubes. Given a Maxwellian population of ions at 2000 km with negligible perpendicular energy, the escaping flux when the potential overcomes gravity is $n_0 v_t B(r)((2\pi)^{1/2}(B_0))^{-1}$. Assuming $T_\parallel$=0.5 eV, evaluating this expression at $r = 2R_E$ on the field line of interest yields $2.7 \cdot 10^4 n_0$ cm^{-2} s^{-1}. When the accelerating potential is changing in time, the fluxes differ from this time stationary value. We have computed numerically the escaping flux of O^+ ions for the distribution functions pictured in Figures 3 and 4. This was done via a trapezoidal integration of $(2\mathcal{E}_\parallel/m_i)^{1/2}$ times the pictured distribution functions. The results are given in Table 2. As a test of the integration method, the upward flux at 1 R_E in the case shown in Figure 2 without a wave present was computed (physically, there is an almost equal downward directed flux in this case). Numerically the upward directed flux is $1.77 \cdot 10^3 n_0$, which compares very well with the theoretical result $1.79 \cdot 10^3 n_0$ found by integrating the product of the velocity and (11), with μ set equal to zero. For the growing wave we find that the escaping flux is enhanced above the time stationary value for the three times shown. This occurs because a growing wave can mix particles of different starting times at 1 R_E altitude. The computed fluxes vary from 26% higher than the time stationary value at 450 s to 18% higher at 1200 s. At late times the flux should asymptote to the time stationary value quoted above. When the wave is decaying, the escaping flux should start at the time stationary value and decrease at later times as the decreasing wave amplitude accelerates fewer O^+ ions. This trend is evident in the last two entries of Table 2. In both cases, the computed escaping fluxes demonstrate the efficiency of a standing wave at dramatically increasing the escaping flux of O^+.

The results presented are for a specific choice of wave model, and do not result in significant transfer of energy into the cyclotron motion of particles about their drifts.

Table 2. Number Flux of Escaping O^+ Ions at 1 R_E Altitude

Time, s	Escaping Flux, n_0 cm^{-2}s^{-1}	Wave Amplitude
450	$3.40 \cdot 10^4$	Growing
900	$3.44 \cdot 10^4$	Growing
1200	$3.21 \cdot 10^4$	Growing
100	$2.17 \cdot 10^4$	Decaying
200	$1.71 \cdot 10^4$	Decaying

Flux computed from the distribution functions pictured in Figures 3 and 4 in terms of the number density of O^+ ions (all with perpendicular energies less than 0.01 eV) at 2000 km altitude, n_0. A Maxwellian with $T_\parallel$=0.5 eV at 2000 km is assumed.

A test calculation with five times the chosen wave frequency did not result in any additional energy in the cyclotron motion. However, when the field line about which the ions gyrate is made a node in the perpendicular direction, that is, the $\cos(k_\alpha(\alpha - \alpha_0))$ replaced by $\sin(k_\alpha(\alpha - \alpha_0))$ in (4), and when a larger electric field amplitude is chosen, jumps in the perpendicular energy are seen when the local oxygen cyclotron frequency is near five and then three times the wave frequency. This effect is subharmonic heating of the ions and has been examined by *Temerin and Roth* [1986] using different numerical techniques. Such heating could substantially change the distribution functions of O^+. The infusion of new perpendicular energy would increase the parallel velocity of O^+ ions as they spiralled up the field lines. The effects of the oscillating parallel electric field on the electrons were also ignored in our study. Depending on the parallel to perpendicular electric field ratio and frequency of the wave, the ponderomotive force on the electrons would result in a different acceleration than that computed here for the ions [*Li and Temerin*, 1993]. This effect would be countered by an ambipolar field that would keep the electrons from running away from the ions. This ambipolar field would make the ion acceleration mass dependent and would result in greater acceleration of oxygen relative to hydrogen. We defer consideration of these additional effects to later studies. As mentioned before, we ignore the normal ambipolar field responsible for the polar wind, which can enhance the relative concentration of H^+ over O^+ at high altitudes, but which should be ignorable compared to the effects of our strong model oscillations.

Conclusions

We have computed the parallel energy distribution function of O^+ ions on an auroral field line at 1 R_E altitude in the presence of a model, standing wave oscillation of the field line at a frequency well below the ion gyrofrequency, assuming a Maxwellian source of ions at 2000 km altitude that has 0.5 eV of thermal energy in the parallel component of velocity and 0.001 eV (negligible) energy in the perpendicular components. The additional effects of a small perpendicular energy were briefly discussed in the text and in Appendix B and were found to be insignificant. The perpendicular electric field had a maximum amplitude of 200 mV m^{-1}, oscillated at 1 Hz, and either grew or decayed in time. The growing wave yielded a parallel distribution function with a broad spectrum of half width 1 to 6 eV that was broader at earlier times; a rounded low-energy cutoff; and a slope at higher energies that asymptoted to $(\log_{10}e)/(2T_\parallel)$, where $T_\parallel$ is the thermal energy of the Maxwellian source. The decaying wave yielded a parallel distribution function with a sharp low-energy cutoff that decreased in energy with increasing time, and had a steeper spectrum at later times. Although the particular value of the slope of the high-energy part of the curves depends upon the assumed distribution function, we would expect similar differences in other distributions in the presence of growing or decaying waves. Within the context of this model the density of upward moving ions at 1 R_E is enhanced above the ambient value by a factor of 2 to 2.6 in the growing wave, given the assumed Maxwellian source at 2000 km altitude. If the $T_\parallel$ of the source in our model is decreased to 0.25 eV, the ambient (no wave present) density at 1 R_E is significantly lowered to $6{\cdot}10^{-4}n_0$ versus $0.0091\ n_0$, but with the wave present the density ratio at 900 s is 58% of that for the 0.5-eV case; the wave manages to bring up comparable amounts of material from sources of both temperatures. The presence of growing or decaying waves can dramatically change the escaping flux of O^+ ions. In a growing wave this escaping flux can for a time exceed the value the escaping flux would reach if the wave had been on for all time. When the wave is decaying, the escaping flux is less than this limiting value. The low-energy cutoff and the location of the peak of the parallel energy distribution versus time give a means of distinguishing the growing wave from the decaying one in terms of the observed parallel distribution function.

Important questions remain to be addressed. One would like to investigate the change in the 3-D distribution induced by the waves. One would also like to know the parallel energy distribution in the presence of a more realistic set of waves: many waves at different discrete frequencies, for example, or a broad spectrum of waves. It would also be of interest to determine how the spectra change when subharmonic heating occurs [*Temerin and Roth*, 1986]. The ambipolar field produced by the different form of the ponderomotive force experienced by electrons versus that exerted on ions [*Li and Temerin*, 1993] should be included. The results presented here, however, give an example of how the distributions and densities of ions can be affected by the presence of Alfvenic oscillations of auroral field lines. Recent Freja observations suggest that such wave structures are a common feature of auroral zone crossings down to even lower altitudes than those studied here, for example, 1700 km [*Louarn et al.*, 1994]. Their resulting ponderomotive acceleration of ionospheric O^+ may contribute to overcoming the gravitational potential energy which would otherwise bind O^+ to lower altitudes, and help to explain the extensive observations of ionospheric O^+ at magnetospheric energies and altitudes in association with enhanced auroral activity.

Appendix A

Figure A1 shows schematically how a point of the parallel velocity distribution is calculated. For purposes of this discussion, positive $v_\parallel$ denotes motion up the field line. Four ions (a, b, c, d) located at about 1 R_E altitude are chosen with different parallel velocities, but with the same gyroenergy and gyrophase. The perpendicular velocities are initialized to the perpendicular drifts from equations (9) and (10), plus whatever perpendicular energy is put into cyclotron motion. These four ions mark the corners of a trapezoidal area in $v_\parallel$-s space, where s is a coordinate along the field line. The

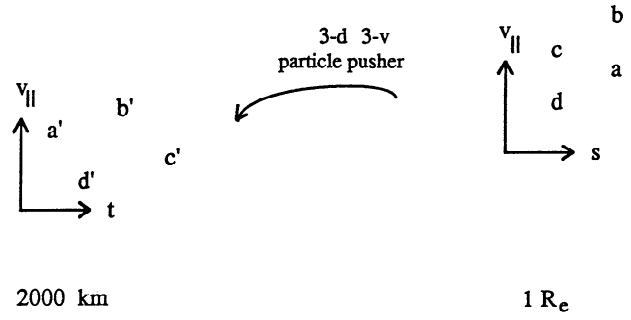

Figure A1. Schematic of how a point of the parallel velocity distribution is calculated for a group of particles with the same perpendicular energy. Four O^+ ions delineating a trapezoidal region of $v_{||}$-s phase space in a region about 1 R_E altitude are pushed back in time until they arrive at 2000 km altitude. Their arrival times and parallel velocities span a region in $v_{||}$-t space at 2000 km altitude where the distribution function is known. An integral of the flux over this region yields the number of particles that occupy the phase volume around 1 R_E altitude, which then allows $\mathbf{f}(v_{||}, 2\ R_E, t)$ to be evaluated.

object is to compute an average distribution function for this region of phase space at time t. The particles are moved backward in time using a Cash-Karp Runge-Kutta scheme [*Press et al.*, 1992], which computes all components of velocity and position. The time the particles reach 2000 km altitude is recorded along with the parallel velocities at the time they reach it. These four times and parallel speeds form a trapezoid in $v_{||}$-t space. An integral of the known parallel flux from the known distribution function (0.5-eV Maxwellian) over this region yields $J(R_E$+2000 km), the number of particles per unit area launched from 2000 km altitude, that cover the phase area of interest around 1 R_E altitude at time t. If $t_{a'}$ is the earliest time at which particles arrive, and $t_{c'}$ is the latest time as is pictured in Figure A1, this integral is

$$J(R_E + 2000\ \text{km}) =$$

$$= \int_{t_{a'}}^{t_{c'}} dt \int_{v_{||}^-(t)}^{v_{||}^+(t)} dv_{||}\ \frac{n_0}{\sqrt{2\pi {v_t}^2}}\, v_{||}\, e^{-v_{||}^2/(2{v_t}^2)}$$

$$= \int_{t_{a'}}^{t_{c'}} dt\ \frac{n_0 v_t}{\sqrt{2\pi}} \left(e^{-v_{||}^-(t)^2/(2{v_t}^2)} - e^{-v_{||}^+(t)^2/(2{v_t}^2)} \right) \quad \text{(A1)}$$

where n_0 is the number density at 2000 km altitude and the double integral is over the trapezoidal region of $v_{||}$-t space pictured in Figure A1. At a given t, $v_{||}^-$ is the lowest parallel velocity on the trapezoid, and $v_{||}^+$ is the highest. As indicated, the integral over parallel velocity can be done explicitly, leaving one dimensional numerical integrals over time to be performed. The location and shape of the trapezoidal region, and therefore J, is determined by how the ions are accelerated between 2000 km and 1 R_E altitudes. The perpendicular area expands as the flux tubes flare, and the ratio of the area at 1 R_E altitude to that at 2000 km altitude is given by the inverse ratio of magnetic field strengths. Given this ratio, the known phase area spanned by the test particles, and the computed number per unit area at 2000 km that were injected up the field line $J(R_E + 2000$ km), the average distribution function at $r = 2R_E$ at time t can be found:

$$f(\bar{v_{||}}, 2R_E, t) =$$

$$J(R_E + 2000\ \text{km}) \cdot \frac{B(2R_E)}{B(R_E + 2000\ \text{km})} \cdot \frac{1}{\sigma(2R_E)} \quad \text{(A2)}$$

where $\bar{v_{||}}$=(sum of four $v_{||}$ values)/4, and $\sigma(2R_E)$ is the area of the trapezoid in $v_{||}$-s space at $r = 2R_E$. In practice, two groups of particles, each with a range of parallel energies and a fixed altitude near 1 R_E, are started on the same field line and propagated backward in time, and the decision on how to group particles is made after they are pushed to 2000 km altitude. A change of variables $\bar{\mathcal{E}}_{||} = 0.5 m_i \bar{v_{||}}^2$ yields the parallel energy distribution function in terms of (A1)

$$F(\bar{\mathcal{E}}_{||}, 2R_E, t) = f\left(\sqrt{2\bar{\mathcal{E}}_{||}/m_i}, 2R_E, t\right) / \sqrt{2 m_i \bar{\mathcal{E}}_{||}} \quad \text{(A3)}$$

As a savings in computer time when the growing wave is assumed, conservation of magnetic moment and gravitational potential energy are used to push ions down to 2000 km altitude if they have not yet reached that altitude by t=0. In this case one needs only to numerically evaluate an integral, and sometimes find a numerical root to an analytical expression. Romberg integration and a bisectional root finder [*Press et al.*, 1992] are employed. Only lower energy particles end up being treated in this manner.

Appendix B

Here a theory is derived for a special case that can be used to check the numerical methods, and can shed light on some of the results. The analysis will first be done for a 3-D velocity distribution. Then, because in this paper a distribution for a fixed value of the final perpendicular energy is computed, a 1-D distribution function for a fixed value of final perpendicular energy (or fixed adiabatic invariant μ) will be found.

Consider a group of O^+ ions moving upwards on a given field line in the presence of a potential energy $U(r)$, which could be the gravitational potential. At 2000 km altitude, $U(r)$ is taken to be zero, and the source distribution is taken to be Maxwellian.

$$f(\mathbf{v}, R_E + 2000\ \text{km})$$

$$= \frac{n_0}{(2\pi {v_t}^2)^{3/2}} e^{-0.5(v_\delta^2 + v_\alpha^2 + v_\phi^2)/{v_t}^2} \quad \text{(B1)}$$

where v_δ, v_α, and v_ϕ are the velocity components in a

dipolar coordinate system, and the thermal energy in each component of velocity is $0.5m_i{v_t}^2$. Assuming that the potential $U(r)$ varies slowly enough with position so that the magnetic moment is conserved, the total energy can be written as

$$\begin{aligned}\mathcal{E}_T &= 0.5m_i(v_\delta^2 + v_\alpha^2 + v_\phi^2) + U(r) \\ &= 0.5m_i v_\parallel^2 + \mu B(r) + U(r) \end{aligned} \quad \text{(B2)}$$

where $v_\parallel = v_\delta$, and $\mu = 0.5m_i(v_\alpha^2 + v_\phi^2)/B$. If f can be written as a function of the total energy, it is a solution to the collisionless Vlasov equation everywhere on the field line. This solution is

$$\mathcal{F}(\mathbf{v}, r) = \frac{n_0}{(2\pi {v_t}^2)^{3/2}} e^{[-0.5m_i v_\parallel^2 - \mu B(r) - U(r)]/(m_i {v_t}^2)} \quad \text{(B3)}$$

where $B_0 = B(R_E + 2000\ \text{km})$, and the parallel energy must satisfy

$$\mathcal{E}_\parallel = 0.5m_i v_\parallel^2 = \max[0., -U(r) - \mu B(r) + \mu B_0] \quad \text{(B4)}$$

Using the change of variables

$$\mathcal{E}_\parallel = 0.5m_i v_\parallel^2, \quad \mu = 0.5m_i(v_\alpha^2 + v_\phi^2)/B(r)$$

the number of particles between $\mathcal{E}_\parallel$ and $\mathcal{E}_\parallel + d\mathcal{E}_\parallel$ and between μ and $\mu + d\mu$ is

$$\frac{d^2 n(\mathcal{E}_\parallel, \mu, r)}{d\mathcal{E}_\parallel d\mu} = \frac{2\pi n_0 B(r)}{(2\pi {v_t}^2)^{3/2}} \frac{e^{-[\mathcal{E}_\parallel + \mu B(r) + U(r)]/(m_i {v_t}^2)}}{\sqrt{2m_i \mathcal{E}_\parallel}} \quad \text{(B5)}$$

where $\mathcal{E}_\parallel$ must still satisfy the constraint (B4).

The value $d\mu$ times the integral of (B5) over the allowed $\mathcal{E}_\parallel$ yields the density of particles between μ and $\mu + d\mu$. Defining $\mathcal{U}_T$ to be

$$\mathcal{U}_T = U(r) + \mu B(r)\left(1 - \frac{B_0}{B(r)}\right) \quad \text{(B6)}$$

$\mathcal{U}_T$ is the effective potential energy difference for motion along the field line; when $r > r_0$, $\mathcal{U}_T > 0$ implies an acceleration of ions down the field line (e.g., gravity), and $\mathcal{U}_T < 0$ implies an acceleration up the field line. The ratio of densities can be written in terms of $\mathcal{U}_T$:

$$\begin{aligned}\frac{n(r,\mu)}{n(R_E + 2000\ \text{km}, \mu)} &= \frac{B(r)}{2B_0} e^{-\frac{\mathcal{U}_T}{m_i {v_t}^2}} \qquad \mathcal{U}_T > 0 \\ \frac{n(r,\mu)}{n(R_E + 2000\ \text{km}, \mu)} &= \frac{B(r)}{2B_0} \text{erfc}\left(\sqrt{\frac{-\mathcal{U}_T}{m_i {v_t}^2}}\right) e^{-\frac{\mathcal{U}_T}{m_i {v_t}^2}} \\ & \qquad \mathcal{U}_T \le 0 \end{aligned} \quad \text{(B7)}$$

where erfc is the complementary error function [*Abramowitz and Stegun*, 1972].

In this paper the parallel distribution function for fixed values of μ is computed, that is, a distribution of particles with the same μ is followed. One can either carry the analysis through by starting with a 1-D Maxwellian and including a $B(r)/B_0$ factor to account for the spreading of the field lines, or one can use the 3-D function (B5) for a small range of μ and normalize the result to the number density at 2000 km found by integrating (B5) over $\mathcal{E}_\parallel$ from zero to infinity. In either case, the result is (11):

$$\frac{dn(\mathcal{E}_\parallel, r, \mu)}{d\mathcal{E}_\parallel} = F(\mathcal{E}_\parallel, r, \mu)$$

$$= \frac{n_0 B(r)}{2B_0\sqrt{2\pi {v_t}^2}} \frac{e^{-[\mathcal{E}_\parallel + \mu B(r) - \mu B_0 + U(r)]/(m_i {v_t}^2)}}{\sqrt{2m_i \mathcal{E}_\parallel}} \quad \text{(B8)}$$

where n_0 is the number density of particles (all with the same μ) at 2000 km altitude. The expression for the density ratio (B7) is unchanged.

Acknowledgments. This work was supported by NASA grants NAGW-1652 and NAG5-1098, and by LACOR contract LANL-UC94-1-A-210. Computations were performed on the SDSC and NASA GSFC Crays.

The Editor thanks W. Allan and S. Ganguli for their assistance in evaluating this paper.

References

Abramowitz, M., and I. A. Stegun (Eds.), *Handbook of Mathematical Functions*, Dover, Mineola, N.Y., 1972.

Allan, W., Ponderomotive mass transport in the magnetosphere, *J. Geophys. Res., 97*, 8483, 1992.

Allan, W., Plasma energization by the ponderomotive force of magnetospheric standing Alfvén waves, *J. Geophys. Res., 98*, 11,383, 1993.

Allan, W., J. R. Manuel, and E. M. Poulter, Does the ponderomotive force move mass in the magnetosphere?, *Geophys. Res. Lett., 17*, 917, 1990.

Allan, W., J. R. Manuel, and E. M. Poulter, Magnetospheric cavity modes: Some nonlinear effects, *J. Geophys. Res., 96*, 11,461, 1991.

Banks, P. M., and T. E. Holzer, High-latitude plasma transport: The polar wind, *J. Geophys. Res., 74*, 6317, 1969.

Chen, F. F, *Introduction to Plasma Physics*, Plenum, New York, 1974.

Guglielmi, A. V., O. A. Pokhotelov, L. Stenflo, and P. K. Shukla, Modifications of the magnetospheric plasma due to ponderomotive forces, *Astrophys. Space Sci., 200*, 91, 1993.

Li, X., and M. Temerin, Ponderomotive effects on ion acceleration in the auroral zone, *Geophys. Res. Lett., 20*, 13, 1993.

Louarn, P., J. E. Wahlund, T. Chust, H. de Feraudy, A. Roux, B. Holback, P. O. Dovner, A. I. Eriksson, and G. Holmgren, Observation of kinetic Alfvén waves by the FREJA spacecraft, *Geophys. Res. Lett., 21*, 1847, 1994.

Lysak, R. L., Theory of auroral zone PiB pulsation spectra, *J. Geophys. Res., 93*, 5942, 1988.

Press, W. H., S. A. Teukolsky, W. T. Vetterling, and B.P. Flannery, *Numerical Recipes in FORTRAN*, 2nd ed., Cambridge University Press, New York, 1992.

Similon, P. L., A. N. Kaufman, and D. D. Holm, Oscillation center theory and ponderomotive stabilization of low-frequency plasma modes, *Phys. Fluids 29*(6), 1908, 1986.

Temerin, M., and I. Roth, Ion heating by waves with frequencies below the ion gyrofrequency, *Geophys. Res. Lett., 13*, 1109, 1986.

M. K. Hudson, X. Li, and E. Witt, Department of Physics and Astronomy, Dartmouth College, Hanover, NH 03755-3528. (email: maryk@comet.dartmouth.edu.)

I. Roth and M. Temerin, Space Sciences Laboratory, Centennial Drive at Grizzly Peak Boulevard, University of California, Berkeley, CA 94720-7450.

(Received July 19, 1994; revised January 13, 1995; accepted January 13, 1995.)